Article

Voronoi Tessellations and the Shannon Entropy of the Pentagonal Tilings

Edward Bormashenko[1]*, Irina Legchenkova[1], Mark Frenkel[1], Nir Shvalb[2], Shraga Shoval[3]

[1] Chemical Engineering Department, Engineering Faculty, Ariel University, P.O.B. 3, 407000 Ariel, Israel
[2] Department of Mechanical Engineering & Mechatronics, Faculty of Engineering, Ariel University, P.O.B. 3, Ariel 407000, Israel
[3] Department of Industrial Engineering and Management, Faculty of Engineering, Ariel University, P.O.B. 3, Ariel 407000, Israel
* Correspondence: edward@ariel.ac.il

Abstract We used the complete set of convex pentagons enabling filing the plane without any overlaps or gaps (including the Marjorie Rice tiles) as generators of Voronoi tessellations. Shannon entropy of the tessellations was calculated. Some of the basic mosaics are flexible and give rise to a diversity of Voronoi tessellations. The Shannon entropy of these tessellations varied in a broad range. Voronoi tessellation, emerging from the basic pentagonal tiling built from hexagons only, was revealed (the Shannon entropy of this tiling is zero). Decagons and hendecagon did not appear in the studied Voronoi diagrams. The most abundant Voronoi tessellations are built from three different kinds of polygons. The most widespread is the combination of pentagons, hexagons and heptagons. The most abundant polygons are pentagons and hexagons. No Voronoi tiling built only of pentagons was registered. Flexible basic pentagonal mosaics give rise to a diversity of Voronoi tessellations, which are characterized by the same symmetry group; however, the coordination number of the vertices is variable. These Voronoi tessellations may be useful for the interpretation of the iso-symmetrical phase transitions.

Keywords: Shannon entropy; pentagonal tiling; Marjorie Rice tiling; Voronoi tessellation; iso-symmetrical transitions.

1. Introduction

The research of families of pentagons admitting tilings (covering) of the plane has a rich and intriguing history. The first five types which admit tile-transitive tessellation of the plane were suggested by Reinhardt [1]. Reinhardt was an assistant of David Hilbert. Hilbert's 18th problem asks whether or not there exist 3-dimensional tiles that admit only non-tile-transitive tessellations. It is customary to think that David Hilbert did not state the 2-dimensional version of this problem as he believed that no such polygons exist [2]. Reinhardt solved Hilbert's 18th problem by demonstrating a 3-dimensional tile that admits only non-tile-transitive tilings of 3D space [2]. However, in the same article, Reinhardt asserted (but did not prove) that a 2D analog does not exist. Heesch demonstrated a counterexample to Reinhardt's suggestion by demonstrating a 2D tile that admits only non-tile transitive tessellation, thus, introducing convex pentagons admitting only non-tile-transitive tilings [2, 3]. Afterwards, Reinhardt himself discovered five pentagonal tessellations of the plane. Additional convex pentagons that admit only non-tile transitive tilings were suggested by Kershner [2, 4]. The set of pentagons enabling the tile-transitive tessellation of the plane were discovered by Marjorie Rice who was an amateur mathematician and mother of five, who had become a follower of Martin Gardner's long-running column, "Mathematical Games", published in the Scientific American magazine [5-6].

The computer classification the convex pentagons that admit paving of the plane was suggested in ref. 2. Exhaustive search of convex pentagons which tile the plane was reported in ref. 7. M. Rao demonstrated that that there are no more than the already 15

 doi:10.20944/preprints202212.0012.v1

known families [7]. We call these families further in the text "basic pentagon tiles", or for sake of brevity "basic tiles" or "basic pentagons".

It seems that the pentagonal tilings resemble the famous Penrose tiling, built from pairs of shapes and demonstrating the 5-fold rotational symmetry [8]. However, actually the pentagonal tilings and Penrose tilings are very different: the Penrose tiling is an example of an aperiodic tiling [9]. In other words, the Penrose tiling represents covering of the plane by non-overlapping polygons, in which shifting any tiling with these shapes by any finite distance, without rotation, cannot produce the same tessellation. The translational symmetry is absent in the Penrose tiling. Contrastingly, the pentagonal tilings, addressed in our paper, are periodic tessellations, characterized by the translational symmetry. Thus, the Penrose and pentagonal tiling represent very different classes of mathematical objects.

Penrose tiling was extremely useful for explanation of the structure of quasi-crystals [10-12]. The very question is: what is the physical exemplification of the pentagonal tiling? We demonstrate that the pentagonal tiling may be used for the explanation of the isosymmetric phase transitions, which were discovered recently [13-16]. The method used in our investigation is based on the building of the Voronoi diagrams on the set of points, emerging from the pentagonal tiling. Vertices of the pentagons are seen as the seed/nuclei points, generating the coressponding Voronoi diagrams (Voronoi tessellations).

Partitioning of an infinite plane into regions based on the distance to a specified discrete set of points (called seeds or *nuclei*) constructs the Voronoi tessellation. There is a corresponding region for each seed, consisting of all points closer to that seed point (also called generators) than to any other point [17-22]. The Voronoi diagram of the addressed Penrose tiling was composed of N polygons. For any given set of points corresponding to the Voronoi tessellation or diagram, the Shannon/Voronoi entropy is defined by Eq. 1:

$$S = -\sum P_n \, ln \, P_n \tag{1}$$

where P_n is the fraction of polygons with n sides or edges (also called the coordination number of the polygon) in a given Voronoi diagram [10-12]. In our paper we analyzed Voronoi tessellations emerging from the 15 known pentagonal tilings. Recently we investigated the Voronoi diagrams generated by the Penrose tiling, and demonstrated fruitfulness of such an analysis [23-24]. The study of the Voronoi diagrams emerging from the pentagonal tilings also supplied non-trivial results.

2. Methods

We studied 15 pentagonal tilings arising from 15 types of basic pentagons, as they were classified in ref. 7. **Figure 1** depicts a pentagonal tile; the edges of the tile are labeled *abcde*, the angles are labeled *ABCDE*.

The basic pentagons, as they were classified in ref. 7, are described in **Table A1**. The majority of these classes allows change in their shape, under variation of their edges and angles; in particular, it is possible to change edges and angles of the classes labeled 1, 2, 3, 4, 5, 6, 7, 8, 9, 10, 11, 12 and 13. These tilings are called in the text "flexible tessellations". Visualization of the change in the shape of the flexible tilings was carried out with the "Tiling Viewer" software by Jaap Scherphuis which can be found on the following link https://www.jaapsch.net/tilings/applet.htm. An example of such a transformation of Tile 11 is shown in **Table 1**.

Preprints (www.preprints.org) | NOT PEER-REVIEWED | Posted: 1 December 2022 doi:10.20944/preprints202212.0012.v1

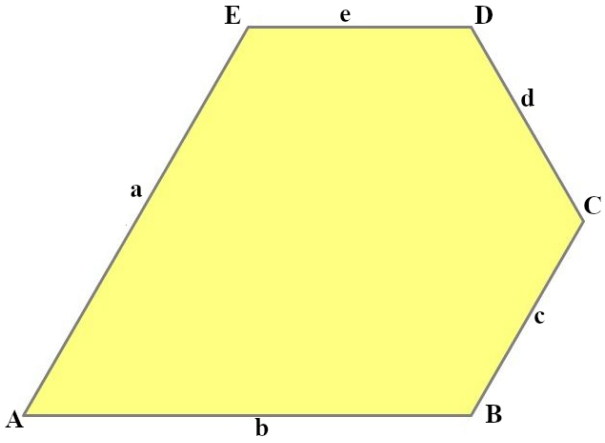

Figure 1. Pentagonal basic tile example with vertices A, B, C, D, E and edges a, b, c, d, and e.

We used 15 tessellations built of pentagons as generators of the Voronoi diagrams (see Column Tiling in **Table A1**). All of the studied pentagon tilings are classified and depicted in **Appendix A** (**Table A1)**. Vertices of the pentagons were used as "seeds" for generation of Voronoi tessellations. Flexible tilings generated a variety of Voronoi diagrams, shown in **Table 1** and **Table A1** (See **Appendix A**). It should be emphasized that the source/basic pentagon-based tilings gave rise to tessellations built of several (from 1 to 5) kinds of polygons to be discussed below. However, no Voronoi tiling built only of pentagons was registered.

3. Results

3.1. Voronoi diagrams generated by the Marjorie Rice Tiling 11

Let us exemplify the suggested approach with the analysis of the Voronoi diagrams emerging from the Marjorie Rice Tiling 11 (see **Table 1**). This tessellation is flexible, and it gives rise to a variety of basic tessellations and correspondingly to the Voronoi diagrams arising from these tessellations.

Let us explain data supplied in **Table 1**. Row 1 supplies the general data related to the basic Marjorie Rice Tiling 11. Small letters (*a*, *b*, *c*) denote edges of the tiling; capitals (*A*, *B*, *C*) denote angles of the tiling. Row 2 of the table depicts the modifications of Tiling 11; row 3 supplies the values of edges and angles for various modifications of Tiling 11. Row 4 depicts the corresponding pentagons, constituting Tiling 11. Row 5 depicts the Voronoi diagrams generated by the vertices of various modifications of Tiling 11. Row 6 supplies the values of the Shannon entropy and parameter ζ defined by Eq. 2. The types of polygons appearing in the Voronoi diagram are also presented in row 6. Angles, denoted *B*, *C*, D and *E*, inherent for Tiling 11, enable variation within [140°;158°], [80°; 44°], [130°;112°], [100°;136°] respectively. Edges *a*, *b* and *c* also enable variation in the flexible Marjorie Rice Tilling 11.

Table 1. Flexible Basic Tile 11 gives rise to various Voronoi tessellations. The values of the Shannon entropy and ratio ζ defined by Eq. 2 are supplied. Color mapping of Voronoi tessellation in row 5 is carried out as follows: green – quadrangles, yellow – pentagons, gray – hexagons, blue – heptagons, orange – octagons, teal – nonagons.

Preprints (www.preprints.org) | NOT PEER-REVIEWED | Posted: 1 December 2022 doi:10.20944/preprints202212.0012.v1

1	Type 11: 2a+c = d=e; A=90°; 2B+C=360°; C+E=180°; (2D+E =360°)		
2	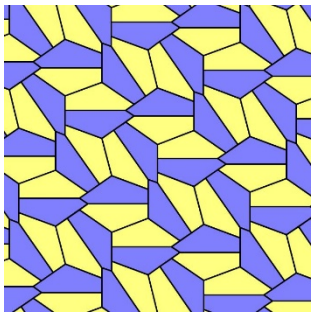	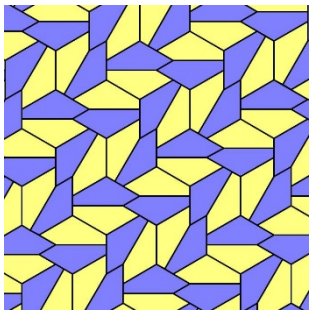	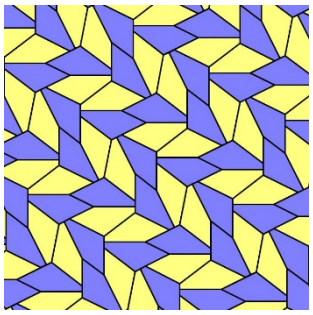
3	A=90°; B=145°; C=70°; D=125°; E=110°; a=28.125, b=116.55; c = 18.75; d=75; e = 75	A=90°; B=150°; C=60°; D=120°; E=120°; a=18.75, b=97.428; c = 37.5; d=75; e = 75	A=90°; B=153.625°; C=52.75°; D=116.375°; E=127.25°; a=11.25, b=79.86; c = 52.5; d=75; e = 75
4	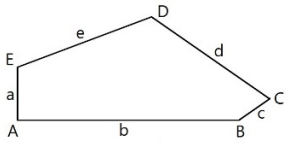	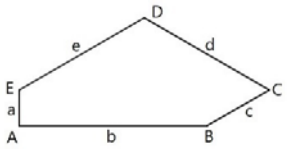	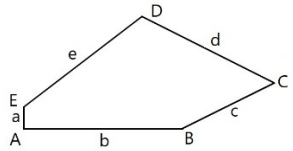
5	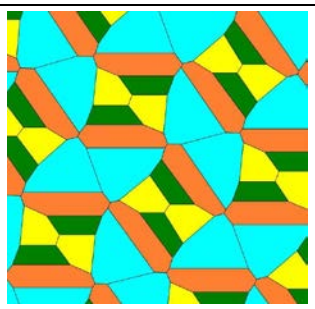	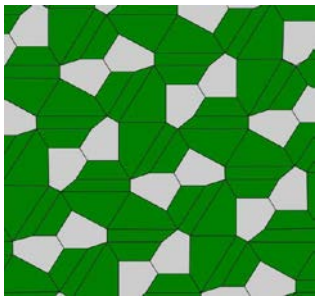	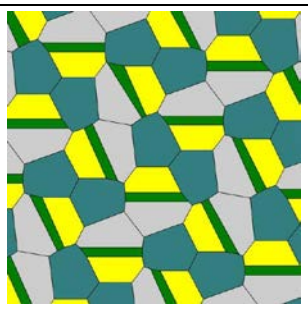
6	4 polygon types: 4, 5, 7,8-vertices ζ=(1:1:1:1) S = 1.386	2 polygon types: 4, 6 -vertices ζ= (3:1) S = 0.562	4 polygon types: 4 5 6 9 -vertices ζ= (1:1:1:1) S = 1.386

The properties of the Voronoi diagrams were quantified with the Shannon entropy calculated with Eq. 1. We also introduced parameter ζ which quantifies the ratio of the number of polygon types appearing in the tiling, defined with Eq. 2, as follows:

$$\zeta = N_k : N_l \ldots : N_z \,,\; k < l < \cdots < z \tag{2}$$

where N_k, N_l and N_z is the number of k, l, and z-edged polygons in an elementary cell of a given Voronoi tiling, k and z are the minimal and maximal number of polygon edges appearing in a given Voronoi tessellation correspondingly.

3.2. Analysis of the Voronoi diagrams emerging from the entire set of basic pentagons

The entire list of the explored source/basic tilings built of pentagons are supplied in **Appendix A (Table A1)**. Vertices of the basic tiles were taken as the seeds of the Voronoi diagrams depicted and characterized in **Table 1** and **Table A1.** The values of the Shannon entropy and ratio ζ for the set of 15 tessellations distinguished by Rao in ref. 7 are supplied in **Table 2**. It is seen from the data supplied in **Table 2**, that various Voronoi diagrams are

Preprints (www.preprints.org) | NOT PEER-REVIEWED | Posted: 1 December 2022 doi:10.20944/preprints202212.0012.v1

characterized by the same values of the Shannon entropy. Thus, Shannon entropies of different Voronoi tessellations may coincide, and this is true even for Voronoi diagrams emerging from various source tessellations.

Obviously, the Shannon entropy of the source tessellation, built of the pentagons only is zero. It is recognized that the Shannon entropy of the Voronoi tessellations is varied in a broad range for the mosaics emerging from the same source pentagonal tiling, namely Eq. 3 is true for Tiling 11:

$$0.562 < S < 1.368 \quad (3)$$

By comparison, for a fully random 2D distribution of points (i.e., with a uniform probability distribution of seed points on a plane), the value of $S = 1.71$ has been reported [21, 24-25].

Table 2. Quantitative parameters of the set of Voronoi tessellations emerging from the 15 basic pentagons. The types of basic pentagons are supplied in **Table A1**. The values the Shannon entropy and parameter ζ defined by Eq. 2 and quantifying the ratio of polygon types which are present in the given tessellation are supplied.

Pentagon type	Voronoi tessellation parameters, S and ratio ζ			
1	2 polygon types: 4 5 ζ=1:1 S = 0.693;	2 polygon types: 5 6 ζ=1:1 S = 0.693;	2 polygon types: 5 8 ζ=2:1 S = 0.637;	
2	2 polygon types: 5 6 ζ=1:1 S = 0.693;	2 polygon types: 4 7 ζ= 1:2 S = 0.637	2 polygon types: 4 8 ζ= 1:1 S = 0.693	2 polygon types: 5 7 ζ= 1:1 S = 0.693
3	3 polygon types: 3 4 6 ζ= 2:3:1 S =1.01	3 polygon types: 3 6 9 ζ= 1:4:1 S = 0.868		
4	2 polygon types: 4 7 ζ= 1:2 S = 0.637	3 polygon types: 4 6 8 ζ= 1:4:1 S = 0.868		
5	3 polygon types: 3 6 7 ζ= 2:1:6 S = 0.849	3 polygon types: 3 5 6 ζ= 2:6:1 S = 0.849	1 type: 6 ζ= 1 S = 0	
6	3 polygon types: 5 6 7 ζ= 1:1:1 S =1.099	3 polygon types: 3 5 6 ζ= 1:1:1 S =1.099		
7	2 polygon types: 5 8 ζ= 1:2 S = 0.637	3 polygon types: 5 6 7 ζ= 1:1 S = 1.099		
8a	2 polygon types: 4 5 ζ= 1:2 S = 0.637	3 polygon types: 5 6 7 ζ= 1:1:1 S = 1.099		

Preprints (www.preprints.org) | NOT PEER-REVIEWED | Posted: 1 December 2022 doi:10.20944/preprints202212.0012.v1

9	3 polygon types: 5 6 7 ζ= 1:1:1 S=1.099			
10	5 polygon types: 4 5 6 7 8 ζ= 2:2:2:4:1 S = 1.516	2 polygon types: 5 12 ζ= 10:1 S = 0.305		
11	4 polygon types: 4 5 7 8 ζ= 1:1:1:1 S = 1.386	4 polygon types: 4 5 6 9 ζ= 1:1:1:1 S = 1.386	2 polygon types: 4 6 ζ= 3:1 S = 0.562	
12	2 polygon types: 5 7 ζ= 1:1 S =0.693	3 polygon types: 4 6 8 ζ=1:3:1 S = 0.950	4 polygon types: 4 5 6 7 ζ= 1:1:1:1 S = 1.386	
13	3 polygon types: 5 6 7 ζ= 2:3:2 S = 1.079	1 type: 6 ζ= 1 S = 0	3 polygon types: 4 5 7 ζ= 1:4:2 S = 0.956	
14	3 polygon types: 5 6 7 ζ= 1:4:1 S = 0.868			
15	3 polygon types: 4 5 6 ζ= 1:2:2 S = 1.055			

Consider that for the plane tiling with the tiles labeled "7-15" the pairs of a pristine pentagon and its mirror reflection were used (see **Table 1A**). These basic tiles may be considered as single-polygon ones, if the pristine pentagon and its mirror reflection are taken as identical polygons. Some of polygons are not flexible; for example, the Rolf Stein tile 14 and Mann/McLoud/Von Derau tile 15 (see **Table 1A**) are rigid and do not enable variation of the geometrical parameters of the pristine pentagons. Thus, they consequently, generate a single type of the Voronoi tessellation (see **Table 1A**). It is noteworthy that the ninth type of tile generated from Marjorie Rice (Tiling 9, see **Table 1a**) also generates a single type of Voronoi tessellations, and this in spite of the fact that this type of tile is flexible and enables change in the shape of pristine pentagons. Basic tile 2 generates the maximal variability of the polygons constituting the Voronoi tessellation (see **Table 2**).

It was established that 15 basic pristine pentagons generate Voronoi diagrams built of eight types of polygons: from triangles to dodecagons. Somewhat surprisingly, decagons and hendecagon do not appear in the Voronoi diagrams. The most astonishing Voronoi tessellation is depicted in **Figure 2**. This tiling, emerging from the basic pentagonal tile of the fifth type, is built from hexagons only.

Preprints (www.preprints.org) | NOT PEER-REVIEWED | Posted: 1 December 2022 doi:10.20944/preprints202212.0012.v1

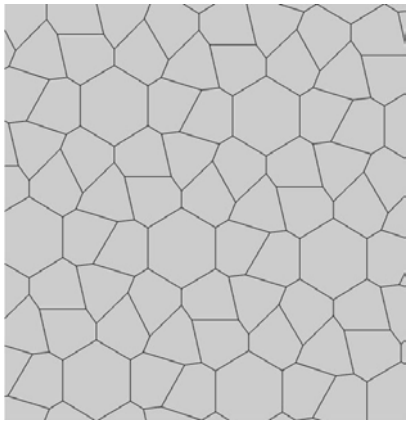

Figure 2. The Voronoi tessellation demonstrating zero Shannon entropy. The tile is generated by the pristine tiling "5" and it is built of hexagons only.

Compare the tiling depicted in **Figure 2** with that built exceptionally of quadrangles, recently reported in ref. 23 and shown in **Figure 3**. The tiling depicted in **Figure 3** emerges from the Penrose P3 tiling, in which the centers of the edges of Penrose P3 rhombs are taken as the seeds (*nuclei*) of the corresponding Voronoi diagram.

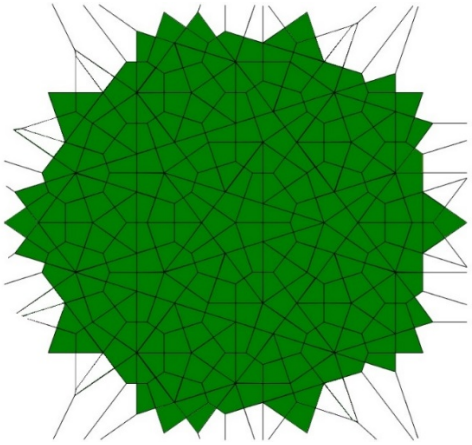

Figure 3. The Voronoi tessellation generated by the Penrose P3 tiling. The centers of the edges of Penrose P3 rhombs are taken as the seeds (*nuclei*) of the Voronoi diagram (for details see ref. 23).

For both of tessellations shown in **Figure 2** and **Figure 3** $S = 0$. Both of tessellations are built from the mix of regular (symmetric) and irregular (non-symmetric) shapes. The Shannon entropy, which usually assumed as a measure of "ordering" in the pattern of the tiling depicted in **Figure 2** is zero. However, it hardly could be agreed, that the pattern, shown in **Figure 2** is strictly ordered. This example supports the idea that the notion of "ordering" has a fine structure and could not be quantified with a single numerical parameter, such as its Voronoi entropy, as already discussed in refs. 23, 24. 26.

It was instructive to study the distribution of polygons in the Voronoi diagrams generated by the basic pentagonal tilings of the plane, summarized in **Table 1A**. As already mentioned the studied Voronoi diagrams may be built from the single type of polygons (hexagons), as shown in **Figure 2**. However, such mono-tilings were rare in occurrence in our investigation. The most abundant tessellations are built from three kinds of polygons

Preprints (www.preprints.org) | NOT PEER-REVIEWED | Posted: 1 December 2022 doi:10.20944/preprints202212.0012.v1

(for example, pentagons, hexagons and heptagons), as shown in **Figures 4-5**. The prevalent polygons are pentagons and hexagons. It should be stressed that no tiling built only of pentagons was registered in our study. It is noteworthy that for the random distribution of seeds the average number of edges surrounding a cell is six in the limit of a large system (provided the averaged coordination number of vertices $\delta = 3$), which is an immediate consequence of Euler's equation in two dimensions, defining the topology characteristics of the surface [19].

Consider the set of Voronoi tessellations, arising from basic pristine pentagons and summarized in **Table 1A**. Let us introduce the parameter K_q (describing the number of Voronoi tessellations K built of q different types of polygons. Actually, parameter q quantifies the variability of polygons within the given Voronoi diagram; the minimal variability of polygons is $q = 1$, which holds for diagrams built of the single type of polygons. In turn, the maximal variability of polygons is $q = 5$, which means that the diagram is built of five types of polygons (the type of a polygon is defined unequivocally by the number of its edges). For example, $K_q = 13_2$ means that that in the entire set of Voronoi tessellations, shown in **Table 1A**, there appear 13 tessellations built of two different types of polygons (for example pentagons and hexagons). The plot depicting the dependence of K_q on the variability q of polygons is supplied in **Figure 4**.

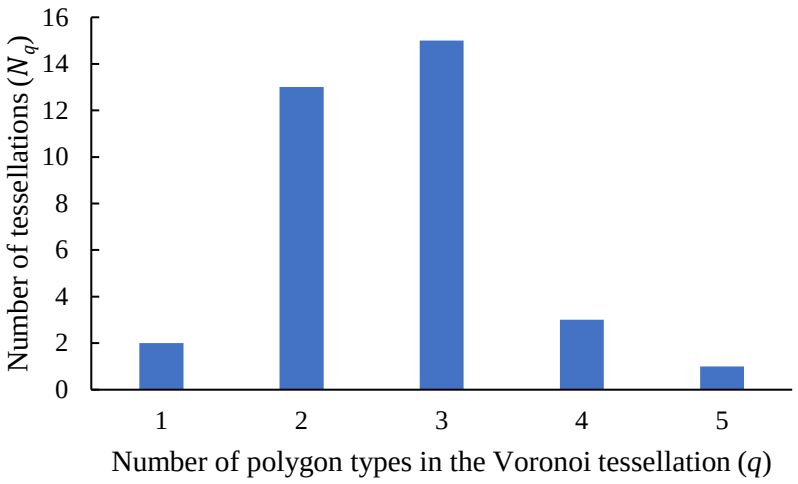

Figure 4. The plot representing the number of Voronoi tessellations N built of q different types of polygons, denoted K_q as a function of number of types of polygons q present in the Voronoi tessellation.

Now let us establish the abundancy of co-occurrence (co-presence) of various polygons within a set of 15 tiles. Various combinations of polygons are present in the investigated Voronoi tessellations, as shown in **Figure 5**. The notation (3,4,6) means that a given Voronoi tessellation is built of polygons with 3, 4, and 6 vertices (triangles, quadrangles and hexagons). **Figure 5** presents the plot of the number of replication of combinations of polygons appearing in the entire set of Voronoi tessellations emerging from 15 types of pentagonal tiling. It is recognized from **Figure 5** that the most abundant is the combination of pentagons, hexagons and heptagons, denoted (5,6,7) and depicted with a green column in **Figure 5**.

Preprints (www.preprints.org) | NOT PEER-REVIEWED | Posted: 1 December 2022 doi:10.20944/preprints202212.0012.v1

The most abundant within the set of Voronoi tessellations generated by 15 basic tiles are pentagons and hexagons as shown in **Figure 6**.

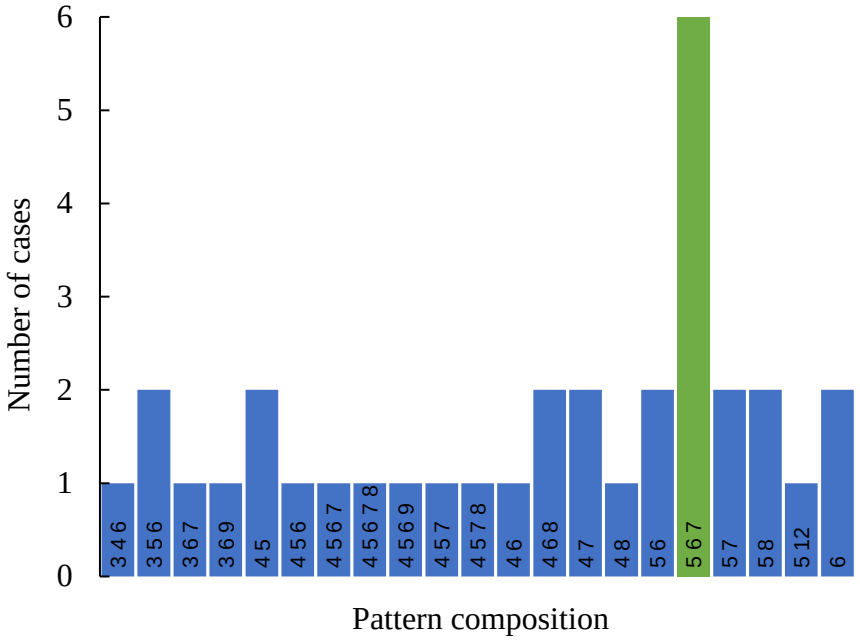

Figure 5. Abundance of appearance of various combinations of polygon types within entire set of investigated Voronoi tessellations. The triad (346) appearing within a column denotes the tessellation built of triangles, quadrangles and hexagons. The number of occurrences of a given combination of polygons is put at the ordinate axis. The most abundant is the (567) combination, i.e. the Voronoi tessellation built of pentagons, hexagons and heptagons, depicted with a green column.

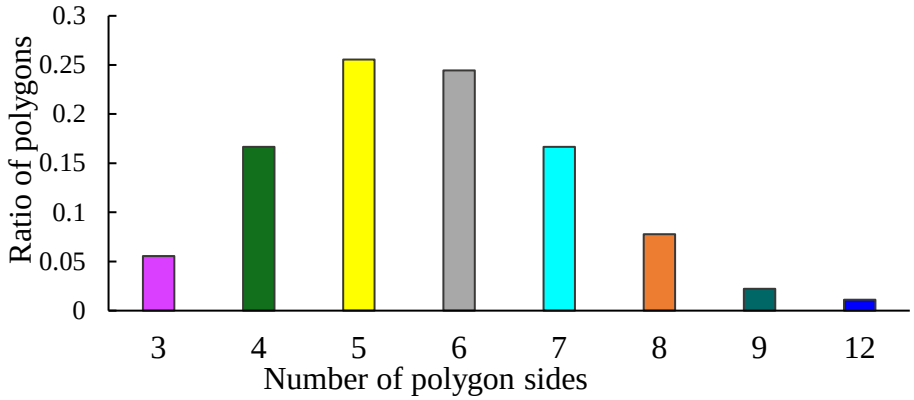

Figure 6. Ratio of polygon types (number of polygon sides $n = 1, 2 \ldots 12$) appearing within the set of Voronoi tessellations generated by the basic tiles. The most abundant are pentagons and hexagons.

Consider now basic tiles № 3, 5, 6, 7, 8, 10, 11, 13. The surprising properties of Voronoi tessellations generated by these basic tiles was revealed. A variety of Voronoi diagrams generated by aforementioned basic tiles, however for all of the Voronoi diagrams Eq. 4 holds:

Preprints (www.preprints.org) | NOT PEER-REVIEWED | Posted: 1 December 2022 doi:10.20944/preprints202212.0012.v1

$$\sum_{i=k}^{i=z} N_i = const \quad (4)$$

where N_i is the number of i-edged polygons in an elementary cell of a given Voronoi tiling, k and z are the minimal and maximal number of polygon edges appearing in a given Voronoi tessellation correspondingly (see Eq. 2).

4. Discussion: Pentagon tilings, Voronoi diagrams and isosymmetric phase transitions

Let us address the following questions why the Voronoi diagrams emerging from pentagon tilings are important? Or, perhaps, these diagrams are of a pure mathematical interest? Is should be emphasized that a set of fifteen tile-transitive basic tiles summarized in **Table 1A** suggest a new kind of spatial ordering of atoms, which may appear in crystals. And this type of ordering is essentially different from that inherent for quasi-crystals, where translational symmetry is absent [10-12]. In contrast, all of basic pentagonal tiles supplied in **Table 1** are characterized by the translational symmetry. But why the Voronoi mosaics generated by the basic tiles are important for physicists? It should be emphasized that Voronoi tessellations of both rigid and flexible basic tiles remain the symmetry of the pristine tiling untouched, as it is recognized from **Table 1A**. However, flexible basic tiles generate plane Voronoi patterns in which the location of vertices is different under keeping the symmetry group of the pattern unaltered (see **Table 1A**). At the same time change in the Voronoi diagram, emerging from the deformation of flexible source pentagons, points to the change of the coordination number of atoms. Such a change in the geometry of the pattern corresponds to the iso-symmetrical phase transitions, which were recently discovered [13-16, 27]. Phase transitions, at which have phases the same space group symmetry are known are iso-symmetric and are necessarily first order. Isosymmetric transitions and/or crossovers occur in important mineralogical systems (pyroxenes, feldspars and carbonates) and non-linear optic materials ($KTiOPO_4$) [13-16, 27].

Conclusions

We investigated properties of the Voronoi tessellations generated by pentagons admitting covering of the plane without gaps and overlapping. The vertices of the basic pentagons were taken as the seeds, generating the Voronoi diagrams. The entire set of these basic polygons includes fifteen types of pentagons, including those introduced by Marjorie Rice. These pentagons are tile-transitive. Some of these pentagons are flexible, i.e. they enable variation of the geometrical parameters: edges and angles. Flexible basic mosaics give rise to a diversity of Voronoi tessellations. The Shannon entropy of these Voronoi tessellations varied in a broad range; for the mosaics emerging from the same source pentagonal tiling (i.e. Tiling 11 supplied in **Table 1A**) we calculated $0.562 < S_{vor} < 1.368$. Somewhat surprisingly, the Voronoi tessellation, emerging from the basic pentagonal tile of the fifth type (see **Table 1A** and **Figure 2**), is built from hexagons only. Consequently, the Shannon entropy calculated for this tiling is zero. Decagons and hendecagons did not appear in the investigated Voronoi diagrams. The most abundant Voronoi tessellations are built from three kinds of polygons (for example, pentagons, hexagons and heptagons). The most widespread is the combination of pentagons, hexagons and heptagons. The most abundant polygons are pentagons and hexagons. It should be stressed, that no Voronoi tiling built only of pentagons was registered in our study. Both basic mosaics and the Voronoi tessellations emerging from basic mosaics are tile-transitive; thus, in principle,

 doi:10.20944/preprints202212.0012.v1

they may describe the planar location of atoms in crystals. Voronoi tessellations keep the symmetry of basic mosaics, however the coordination number of vertices may be changed for the flexible patterns. Flexible basic pentagonal mosaics give rise to a diversity of Voronoi tessellations which are characterized by the same symmetry group. Thus, these Voronoi tessellations may be useful for the interpretation of the iso-symmetrical phase transitions.

Author Contributions: Conceptualization, M.F. and E.B.; methodology, I. L., M. F. and E. B.; software, M. F. and I.L.; validation, S.S. and N. S; formal analysis, M. F., E. B., I.L., S. S. and N. S.; investigation, M. F. and I. L.; writing—original draft preparation, E.B. and M.F.; supervision, S. S. and N. S. All authors have read and agreed to the published version of the manuscript.

Funding: This research received no external funding.

Institutional Review Board Statement: Not applicable.

Data Availability Statement: Not applicable.

Acknowledgments: In this section, you can acknowledge any support given which is not covered by the author contribution or funding sections. This may include administrative and technical support, or donations in kind (e.g., materials used for experiments).

Conflicts of Interest: The authors declare no conflict of interest.

References

1. Reinhardt, K.: Über die zerlegung der ebene in polygone. Ph.D. thesis, Univ. Frankfurt a. M. Noske (1918).
2. Mann, C.; McLoud-Mann, J.; Von Derau, D. Convex pentagons that admit i-block transitive tilings. *Geom Dedicata* **2018**, *194*, 141–167.
3. Heesch, H.: Aufbau der ebene aus kongruenten bereichen. *Nachr. Ges. Wiss. Göttingen New Ser*. **1935**, *1*, 115–117.
4. Kershner, R. B. On paving the plane. *Am. Math. Mon*. **1968**, *75*, 839–844.
5. Schattschneider, D. Marjorie Rice (16 February 1923–2 July 2017), J. Mathematics & Arts, **2018**, *12* (1), 51-54.
6. Schattschneider, D. Marjorie Rice and the MAA tiling, Journal of Mathematics and the Arts, **2018**, *12* (2-3), 114-127,
7. Rao, M. Exhaustive search of convex pentagons which tile the plane, **2017**, arXiv: 1708.00274.
8. Penrose, R. Pentaplexity A Class of Non-Periodic Tilings of the Plane. *The Mathematical Intelligencer* **1979**, *2*, 32–37.
9. Macia, E. The role of aperiodic order in science and technology. *Rep. Prog. Phys*. *2005*, *68*, 1–45.
10. Shechtman, D.; Blech, I.; Gratias, D.; Cahn, J.W. Metallic phase with long-range orientational order and no translational symmetry. *Phys. Rev. Lett*. **1984**, *53*, 1951–1953.
11. Collins, L.C.; Witte, T.G.; Silverman, R.; Green, D.B.; Gomes, K.K. Imaging quasiperiodic electronic states in a synthetic Penrose tiling. *Nat. Commun*. **2017**, *8*, 15961.
12. Bursill, L.; Ju Lin, P. Penrose tiling observed in a quasi-crystal. *Nature* **1985**, *316*, 50–51.
13. A. J. Hatt, N. A. Spaldin, Strain-induced isosymmetric phase transition in $BiFeO_3$, *Phys. Rev. B* **2010**, *81*, 054109.
14. J. Haines, J. M. Léger, and O. Schulte, High-pressure isosymmetric phase transition in orthorhombic lead fluoride. *Phys. Rev. B* **1998**, *57*, 7551.
15. S. M. Clarke, B. A. Steele, M. P. Kroonblawd, D. Zhang, I-F. W. Kuo, E. Stavrou, An Isosymmetric High-Pressure Phase Transition in α-Glycylglycine: A Combined Experimental and Theoretical Study. *J. Phys. Chem*. B **2020,** *124*, 1, 1–10.
16. A. Liang, C. Popescu, F. J. Manjon, R. Turnbull, E. Bandiello, P. Rodriguez-Hernandez, A. Muñoz, I. Yousef, Z. Hebboul, D. Errandonea, Pressure-Driven Symmetry-Preserving Phase Transitions in $Co(IO_3)_2$. *J. Phys. Chem. C* **2021**, *125*, 17448−17461.
17. Voronoi, G. Nouvelles applications des paramètres continus à la théorie des formes quadratiques. Deuxième mémoire. Recherches sur les parallélоèdres primitifs. *Reine Angew. Math*. **1908**, *134*, 198–287.
18. Barthélemy, M. Spatial networks. *Phys. Rep*. **2011**, *499*, 1–101.
19. Weaire, D.; Rivier, N. Soap, cells and statistics—random patterns in two dimensions. *Contemp. Phys*. **1984**, *25*, 59–99.
20. Xu, K. Geometric formulas of Lewis's law and Aboav-Weaire's law in two dimensions based on ellipse packing, *Phil. Mag. Lett*. **2019**, *99* (9), 317-325.

 doi:10.20944/preprints202212.0012.v1

21. Bormashenko, E.; Frenkel, M.; Vilk, A.; Legchenkova, I.; Fedorets, A.A.; Aktaev, N.E.; Dombrovsky, L.A.; Nosonovsky, M. Characterization of self-assembled 2D patterns with Voronoi Entropy. *Entropy* **2018**, *20*, 956.
22. Lopez-Sauceda, J.; von Bülow, P.; Ortega-Laurel, C.; Perez-Martinez, F.; Miranda-Perkins, K.; González, J.G.C. Entropy as a Geometrical Source of Information in Biological Organizations, *Entropy* **2022**, *24*(10), 1390.
23. Bormashenko, E.; Legchenkova, I.; Frenkel, M.; Shvalb, N.; Shoval, S. Voronoi Entropy vs. Continuous Measure of Symmetry of the Penrose Tiling: Part I. Analysis of the Voronoi Diagrams. *Symmetry* **2021**, *13*, 1659.
24. Bormashenko, Ed.; Legchenkova, I.; Frenkel, M.; Shvalb, N.; Shoval, Sh. Informational Measure of Symmetry vs. Voronoi Entropy and Continuous Measure of Entropy of the Penrose Tiling. Part II of the "Voronoi Entropy vs. Continuous Measure of Symmetry of the Penrose Tiling. Symmetry **2021**, *13* (11), 2146.
25. Limaye, A.V.; Narhe, R.D.; Dhote, A.M.; Ogale, S.B. Evidence for convective effects in breath figure formation on volatile fluid surfaces. *Phys. Rev. Lett*. **1996**, *76*, 3762–3765.
26. Bormashenko, Ed.; Legchenkova, I.; Frenkel, M. Shvalb, N.; Shoval, Sh. Shannon (Information) Measures of Symmetry for 1D and 2D Shapes and Patterns. *Appl. Sci*. **2022**, *12*(3), 1127.
27. Christy, A. G. Isosymmetric structural phase transitions: phenomenology and examples. *Acta Cryst. B* **1995**, *51*, 753-757.

Appendix A

Table A1. 15 types of basic tiles (column Tilling) and corresponding Vornoi tessellations generated by the basic tiles (columns Voronoi tessellations). The Voronoi entropy of the patterns and the values of parameter ζ, defined by Eq. 2, are supplied Coloring of the patterns: triangles – purple, quadrangles – green, pentagons – yellow, hexagons – grey, heptagons – blue, octagons – orange, nonagons – teal, dodecagons – deep blue.

Type	Tiling	Voronoi tessellation	
1	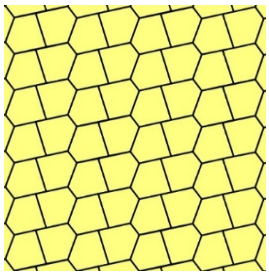 $B+C=180$ ($A+D+E=360°$)	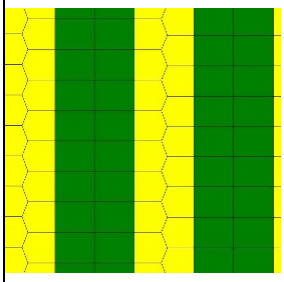 2 types: 4 5 $S = 0.693$; ζ=(1:1)	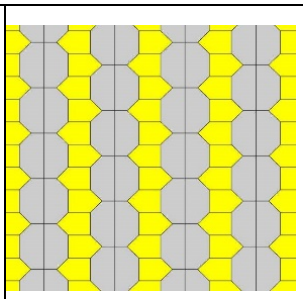 2 types: 5 6 S=0.693; ζ=(1:1)
		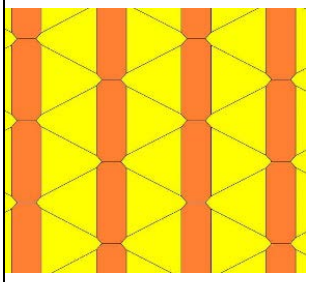 2 types: 5 8 S=0.637; ζ=(2:1)	

Preprints (www.preprints.org) | NOT PEER-REVIEWED | Posted: 1 December 2022 doi:10.20944/preprints202212.0012.v1

2	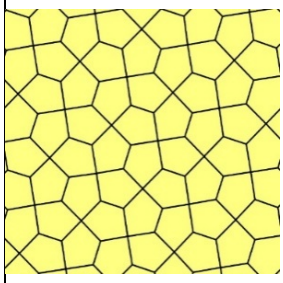 *c*=*e* *B*+*D*=180° (*A*+*C*+*E*=360°)	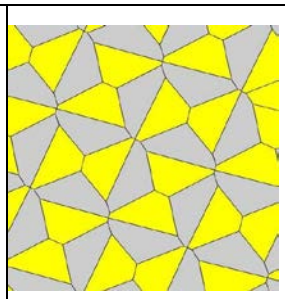 2 types: 5 6 *S*=0.693; ζ =(1:1)	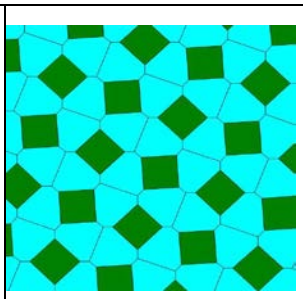 2 types: 4 7 *S*= 0.637; ζ =(1:2)
		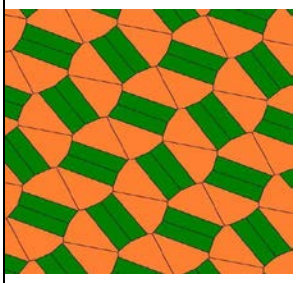 2 types: 4 8 *S*= 0.693; ζ= (1:1)	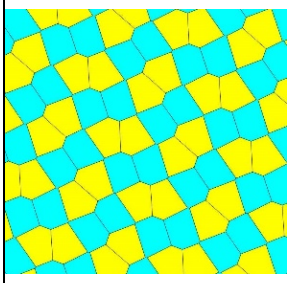 2 types: 5 7 *S*=0.693; ζ = (1:1)
3	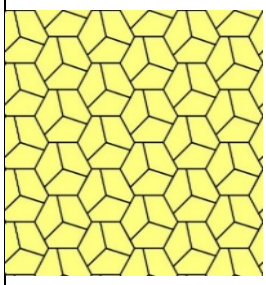 *a*=*b*, d=*c*+*e* *A*=*C*=*D*=120° (*B*+*E*=180°)	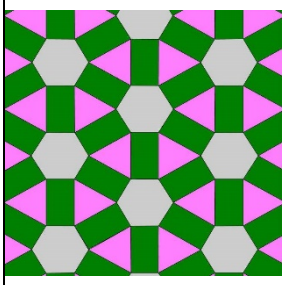 3 types: 3 4 6 *S*=1.011; ζ= (2:3:1)	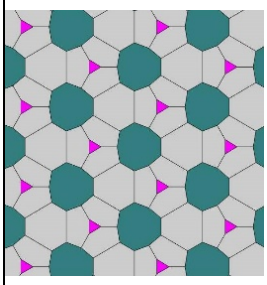 3 types: 3 6 9 *S*= 0.868; ζ= (1:4:1)
4	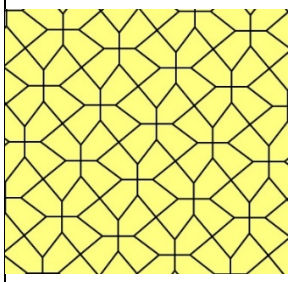 *b*=*c*, *d*=*e*, *B*=90°, *D*=90° (*A*+*C*+*E*=360°)	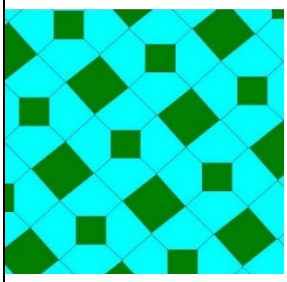 2 types: 4 7 *S*= 0.637; ζ= (1:2)	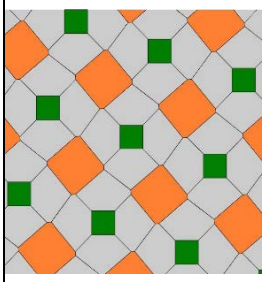 3 types: 4 6 8 *S*= 0.868; ζ= (1:4:1)

Preprints (www.preprints.org) | NOT PEER-REVIEWED | Posted: 1 December 2022 doi:10.20944/preprints202212.0012.v1

5	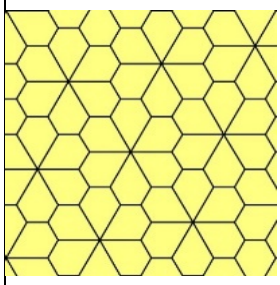 *a*=*b*, *d*=e, *A*=60° *D*=120° (*B*+*C*+*E*=360°)	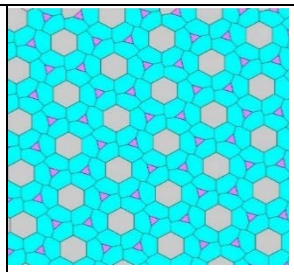 3 types: 3 6 7 *S* = 0.849; *ζ*= (2:1:6) 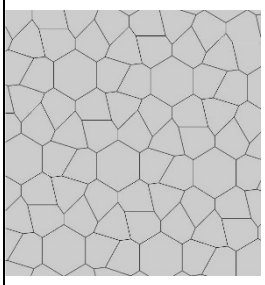 1 type: 6; *S* = 0 (1)	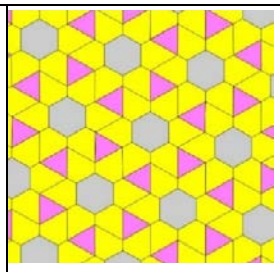 3 types: 3 5 6 *S* = 0.849; *ζ*= (2:6:1)
6	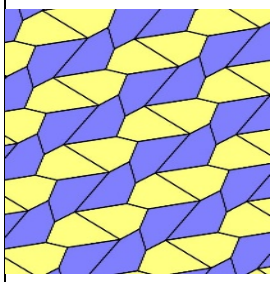 *a*=*d*=*e*, *b*=*c* *B*+*D*=180°, 2*B*=*E* (*A*+*C*+*E*=360°)	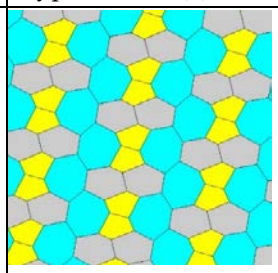 3 types: 5 6 7 *S* =1.099; *ζ*= (1:1:1)	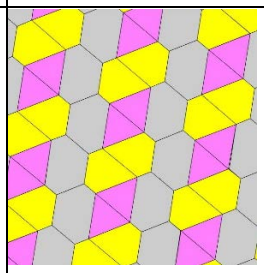 3 types: 3 5 6 *S* =1.099; *ζ*= (1:1:1)
7	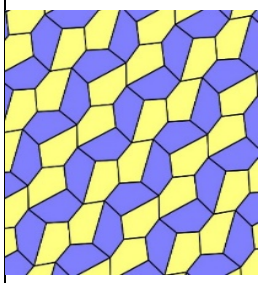 *b*=*c*=*d*=*e* *B*+2*E*=360°, 2*C*+*D*=360° (2*A*+*B*+*D*=360°)	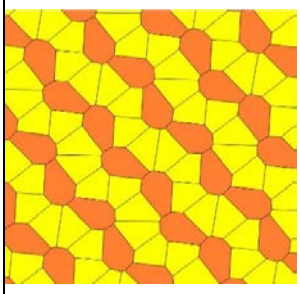 2 types: 5 8 *S* = 0.637; *ζ*= (1:2)	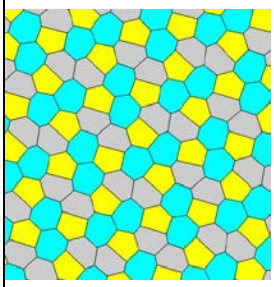 3 types: 5 6 7 *S* = 1.099; *ζ*= (1:1:1)
8a	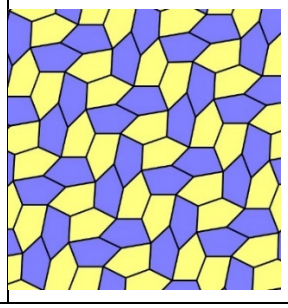	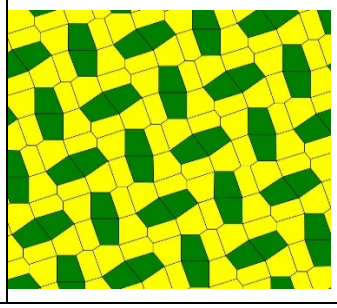	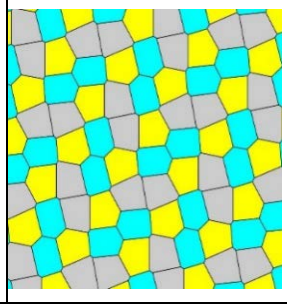

Preprints (www.preprints.org) | NOT PEER-REVIEWED | Posted: 1 December 2022 doi:10.20944/preprints202212.0012.v1

	b=*c*=*d*=*e* 2*B*+*C*=360°, *D*+2*E*=360° (2*A*+*C*+*D*=360°)	2 types: 4 5 *S* = 0.637; ζ = (1:2)	3 types: 5 6 7 *S* = 1.099; ζ = (1:1:1)
9	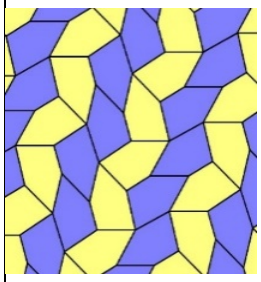 *b*=*c*=*d*=e 2*A*+*C*=360°, *D*+2*E*=360° (2*B*+*C*+*D*=360°)	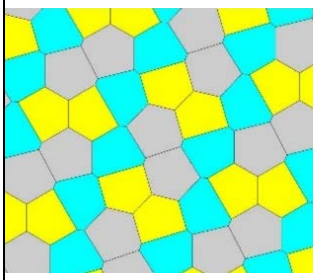 3 types: 5 6 7 *S* =1.099; ζ = (1:1:1)	
10	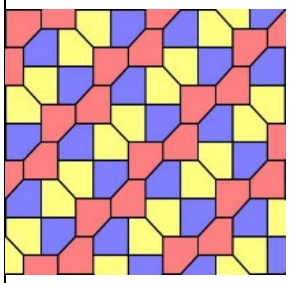 *a*=*b*=*c*+*e* *A*=90°, *B*+*E*=180°, *B*+2*C*=360°; (*C*+*D*=270°)	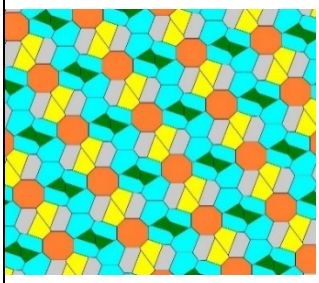 5 types: 4 5 6 7 8 *S* = 1.516; ζ = (2:2:2:4:1)	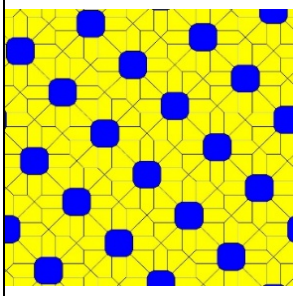 2 types: 5 12 *S* = 0.305; ζ = (10:1)
11	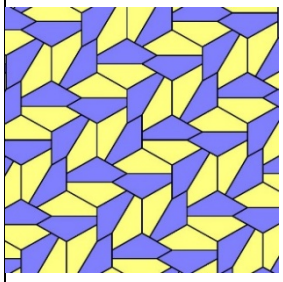 2*a*+*c*=*d*=*e* *A*=90°, 2*B*+*C*=360°, *C*+*E*=180° 2*D*+*E*=360°	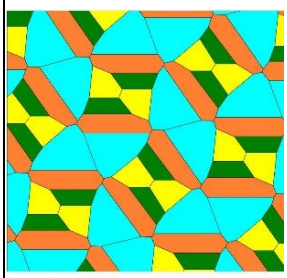 4 types: 4 5 7 8 *S* = 1.386; ζ = (1:1:1:1) 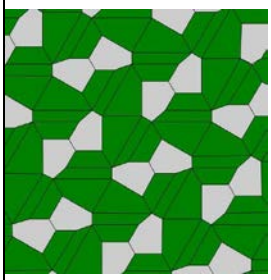 2 types: 4 6; *S* = 0.562; ζ = (3:1)	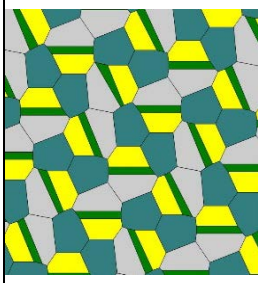 4 types: 4 5 6 9 *S* = 1.386; ζ = (1:1:1:1)

Preprints (www.preprints.org) | NOT PEER-REVIEWED | Posted: 1 December 2022 doi:10.20944/preprints202212.0012.v1

12	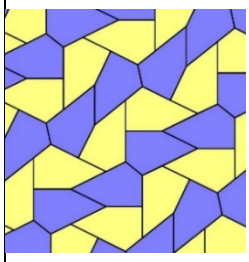 $2a=d=c+e$ $A=90°$, $2B+C=360°$, $C+E=180°$ $2D+E=360°$	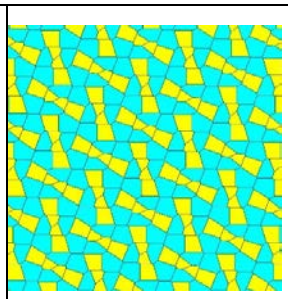 2 types: 5 7 $S=0.693$; $\zeta=(1:1)$	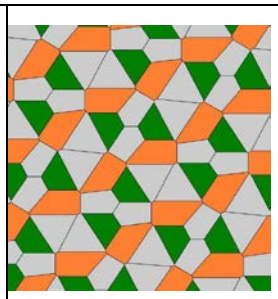 3 types: 4 6 8 $S=0.950$; $\zeta=(1:3:1)$
		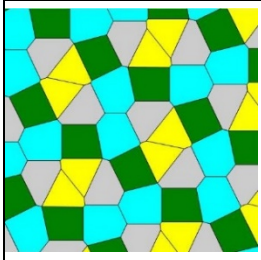 4 types: 4 5 6 7 $S=1.386$; $\zeta=(1:1:1:1)$	
13	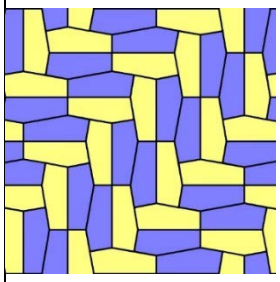 $d=2a=2e$ $B=E=90°$, $2A+D=360°$ $2C+D=360°$	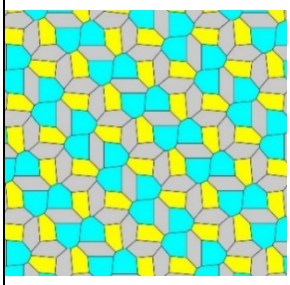 3 types: 5 6 7 $S=1.079$ (2:3:2)	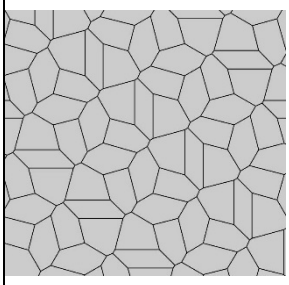 1 type: 6 $S=0$ (1)
		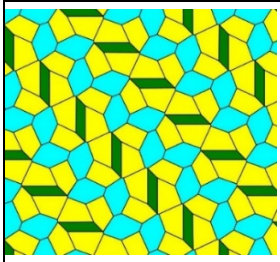 3 types: 4 5 7; $S=0.956$; $\zeta=$ (1:4:2)	
14	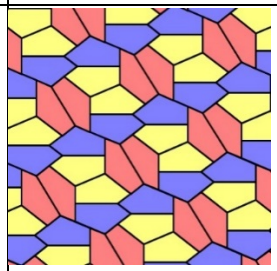 $2a=2c=d=e$ $A=90$, $2B+C=360°$, $C+E=180°$; $(2D+E=360°)$	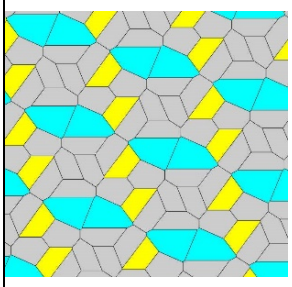 3 types: 5 6 7 $S=0.868$; $\zeta=(1:4:1)$	

Preprints (www.preprints.org) | NOT PEER-REVIEWED | Posted: 1 December 2022 doi:10.20944/preprints202212.0012.v1

15	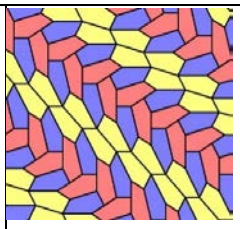 *a*=*c*=*e*, b=2*a* *A*=*D*=105°, *B*=60°, *C*=13°5 (*E*=90°)	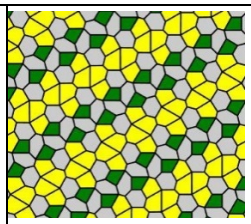 3 types: 4 5 6 *S* = 1.055; ζ = (1:2:2)	